

Graphene synthesized in atmospheric plasmas—A review

Albert Dato^{a)}

Department of Engineering, Harvey Mudd College, Claremont, California 91711, USA

(Received 1 June 2018; accepted 30 November 2018)

This article reviews the state of the art in the gas-phase synthesis of graphene in atmospheric plasmas. The substrate-free process involves the delivery of a carbon-containing precursor into a microwave-generated Ar plasma. Factors that influence the synthesis of graphene include precursor composition, reactor design, and the flow rates of gases. These factors have elucidated the mechanisms of graphene formation in atmospheric plasmas. Gas phase-synthesized graphene is pure and highly ordered and possesses unique features that make the material useful in applications such as catalysis, energy storage, lubrication, and the transmission electron microscopy imaging of nanomaterials. However, the main challenge in the synthesis process is the low rate of graphene production. This article anticipates future research aimed at overcoming this challenge and compares the atmospheric plasma method with contemporary graphene production techniques.



Albert Dato

Albert Dato is the Iris and Howard Critchell Assistant Professor at Harvey Mudd College. He received his B.S. degrees in Mechanical Engineering and Aeronautical Engineering from UC Davis in 2001. Under the mentorship of Professor Michael Frenklach, he received his M.S. degree in Mechanical Engineering in 2004 and Ph.D. in Applied Science & Technology in 2009 from UC Berkeley. He discovered the substrate-free gas-phase synthesis of graphene in atmospheric plasmas at UC Berkeley. After receiving his Ph.D., he worked as a process development engineer at Novellus Systems Inc., where he developed high-density plasma chemical vapor deposition processes for semiconductor device fabrication. He also worked as a scientist at Air Liquide Electronics US LP, where he led the research and development of new products, processes, and services for detecting and analyzing nanoscale contamination on high-performance materials used throughout the semiconductor industry. Driven by his passions for teaching, scientific research, and increasing diversity in STEM, he joined the faculty of Harvey Mudd College in 2014. He currently directs the Energy and Nanomaterials Lab at Harvey Mudd College, and his research focuses on developing solutions to energy and environmental challenges through the synthesis and applications of advanced materials.

I. INTRODUCTION

Graphene is a single layer of sp^2 -bonded carbon atoms arranged in a honeycomb structure (Fig. 1). A pristine graphene sheet has a Young's modulus of 1000 GPa^{1,2} and an ultimate tensile strength of 130 GPa.¹ For comparison, A36 steel exhibits a Young's modulus of 200 GPa³ and an ultimate tensile strength of 0.4 GPa.^{3,4} The thermal conductivity of the two-dimensional material is greater than 3000 W/(m K) near room temperature,^{5,6} and the electron mobility of suspended graphene sheets is as high as 200,000 cm²/(V s) at low temperatures.^{7,8}

Graphene powder has numerous applications. For example, multifunctional polymer-matrix nanocomposites with enhanced mechanical,⁹ electrical,^{10,11} and thermal¹² properties have been fabricated using graphene

powder as a filler. Friction tests have revealed that lubricant oils containing graphene powder have significantly lower wear and coefficient of friction than oils containing graphite or carbon black.¹³ Flexible displays¹⁴ and chemical sensors¹⁵ can be created using electrically conductive inks containing graphene powder.^{16–18} Additionally, extensive research has been conducted on the use of graphene powder in energy storage applications,^{19,20} such as lithium-ion batteries^{20–22} and capacitors.^{23,24}

Pure and highly ordered graphene powder can be continuously synthesized in the gas phase using atmospheric plasmas. This single-step process occurs at ambient conditions, without the use of substrates, catalysts, solvents, or acids. The objective of this review is to increase the awareness and understanding of gas phase-synthesized graphene (GSG). This article will present the research conducted on GSG and the current understanding of the mechanisms of GSG formation in atmospheric plasmas. This paper will also discuss the challenge of low

^{a)}Address all correspondence to this author.
e-mail: adato@hmc.edu
DOI: 10.1557/jmr.2018.470

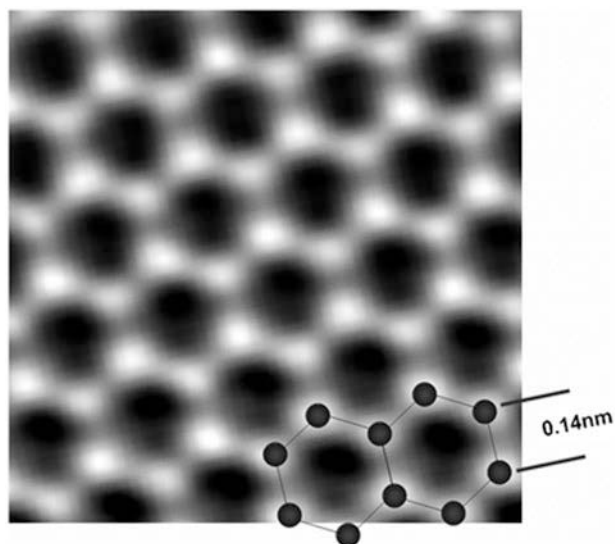


FIG. 1. An atomic resolution image of a clean and structurally perfect graphene sheet synthesized in an atmospheric plasma. Individual carbon atoms appear white in the image. The image was obtained through the reconstruction of the electron exit wave function from 15 lattice images using MacTempas Version 2 software. Reproduced from Ref. 36 with permission from the Royal Society of Chemistry. MacTempas is developed by Total Resolution LLC, Berkeley, CA, USA.

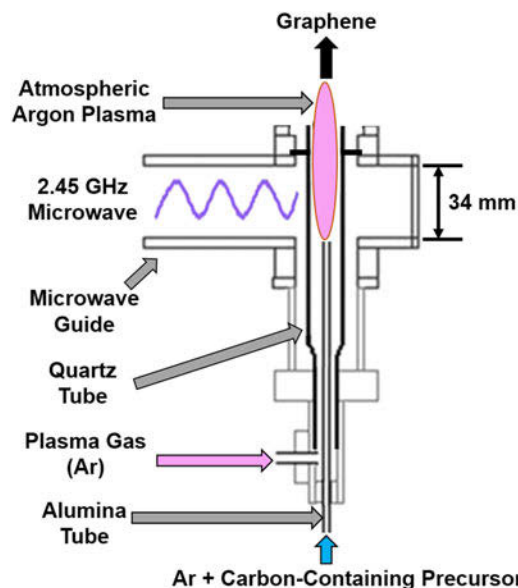


FIG. 2. Schematic of an atmospheric pressure microwave plasma reactor used to produce GSG.

GSG production rate and will anticipate future research that could potentially overcome this challenge. Furthermore, the structure, composition, features, and applications of GSG will be highlighted. The production of GSG will then be compared with other methods of obtaining graphene, including plasma-enhanced chemical vapor deposition (PECVD), micromechanical cleavage, the reduction of graphene oxide, and the liquid-phase exfoliation of graphite.

II. ATMOSPHERIC PLASMA SYNTHESIS OF GRAPHENE

The production of GSG involves the delivery of a carbon-containing precursor, such as ethanol, into an atmospheric pressure microwave-generated Ar plasma^{25,26} (Fig. 2). Precursors enter the region of the plasma where microwave power is absorbed by the plasma electrons (this region is hereafter referred to as the coupler region). Plasma electrons transfer energy to heavy particles (ions and neutral atoms) through elastic and inelastic collisions in the coupler region, which is an environment that has an electron density $\geq 10^{13} \text{ cm}^{-3}$ and gas temperatures as high as 3000 K.^{27–29} Precursors that enter the coupler region are decomposed into smaller reactive fragments, such as C, H, H₂, C₂, C₂H₂, and CO.^{27–31} These reactive fragments then flow out of the coupler region and into the plasma afterglow, where they react to form nuclei that rapidly grow into GSG.^{26,29} The entire process of precursor delivery, decomposition, and GSG formation takes place over a time period on the order of 10^{-1} s .^{25,28} GSG sheets exit the plasma afterglow and are typically collected downstream from the plasma on filters.^{25,28}

A number of materials characterization techniques have shown that GSG powder is highly ordered and pure. Low-magnification transmission electron microscopy (TEM) images have revealed that the synthesized powder consists of crumpled and randomly oriented sheets [Fig. 3(a)]. Results from the electron energy loss spectroscopy (EELS) characterization of GSG show a peak at 285 eV that corresponds to transitions from the 1 s to the π^* states and a peak at 291 eV that corresponds to transitions from the 1 s to the σ^* states [Fig. 3(b)].^{32–35} These peaks are characteristic of graphite and graphene. High-magnification TEM images of GSG have shown that the synthesized powder consists of monolayer and few-layer sheets [Fig. 4(a)]. The aberration-corrected TEM image shown in Fig. 1 demonstrates that GSG has a highly ordered two-dimensional honeycomb lattice of carbon atoms, which is characteristic of pristine graphene.³⁶ The Raman spectrum of GSG shown in Fig. 4(b) exhibits peaks that are characteristic of graphene, such as a sharp, symmetric 2D peak at $\sim 2660 \text{ cm}^{-1}$, which is the second order of zone-boundary phonons³⁷; a G peak at $\sim 1580 \text{ cm}^{-1}$, which is due to the doubly degenerate zone center E_{2g} mode^{37,38}; and a peak at $\sim 1350 \text{ cm}^{-1}$ called the D peak,^{37,38} which is caused when edges of GSG are captured in a Raman laser spot.³⁹

GSG has a mass composition of 98.9% C, 1.0% H, and 0.1% O, as determined by elemental analysis by combustion.³⁶ The Fourier transform infrared spectroscopy and X-ray photoelectron spectroscopy results shown in Fig. 5 provide additional evidence that the purity of GSG

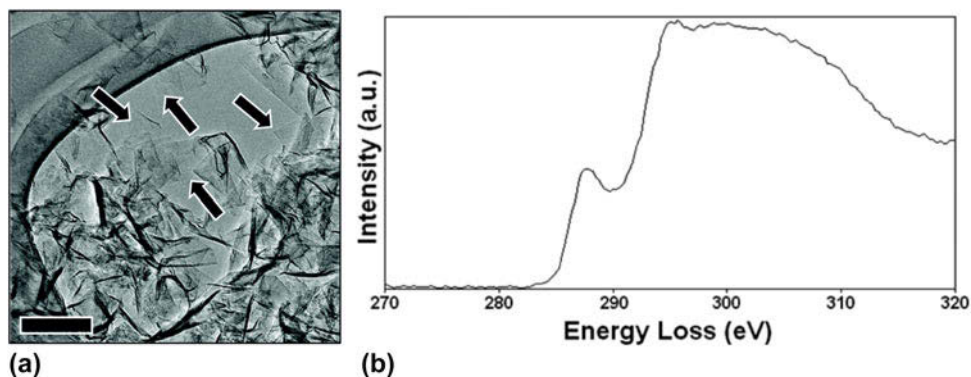


FIG. 3. (a) A typical low-magnification TEM image of crumpled and randomly oriented GSG sheets freely suspended on a lacey carbon TEM grid. Homogeneous and featureless regions (indicated by arrows) indicate regions of monolayer graphene. Scale bar represents 100 nm. (b) EELS spectrum of GSG. Reprinted (adapted) with permission from Dato et al.: Substrate-free gas-phase synthesis of graphene sheets. *Nano Lett.* 8, 2012 (2008). Copyright 2008 American Chemical Society.

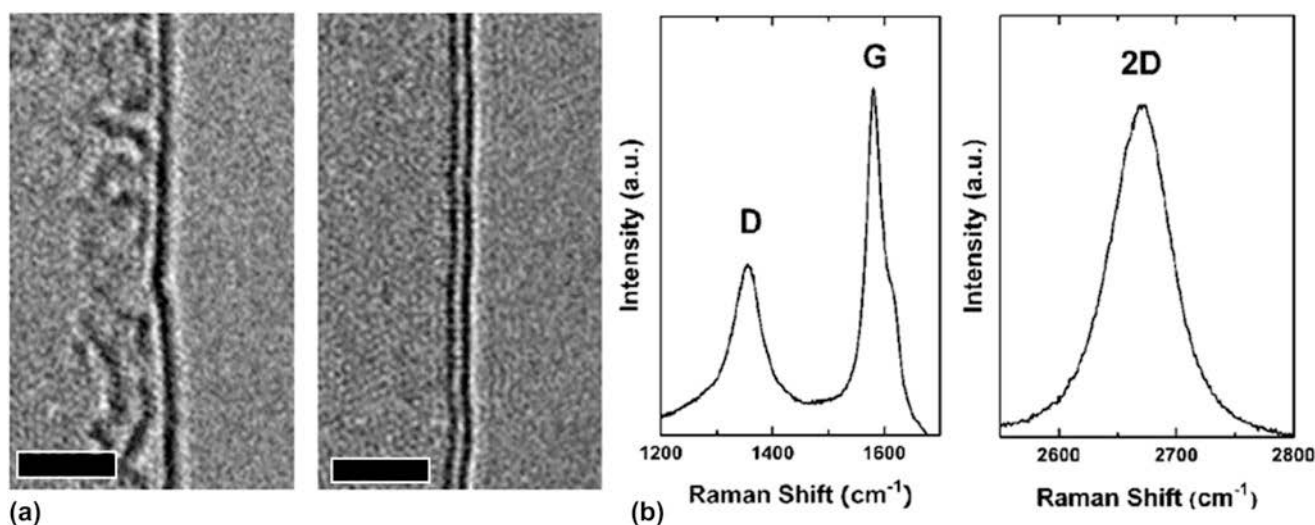


FIG. 4. (a) High-magnification image of single-layer and bilayer GSG. Scale bars represent 2 nm. (b) Raman spectrum of GSG. Reprinted with permission from Dato et al.: Substrate-free gas-phase synthesis of graphene sheets. *Nano Lett.* 8, 2012 (2008). Copyright 2008 American Chemical Society.

is similar to highly oriented pyrolytic graphite (HOPG), which is 99.9% C. Thus, GSG is similar to the high-quality graphene specimens obtained through the micro-mechanical cleavage of HOPG.^{37,40}

III. FACTORS THAT INFLUENCE GRAPHENE SYNTHESIS IN ATMOSPHERIC PLASMAS

A. Reactor design, pressure, and microwave forward power

The production of GSG was first achieved using the atmospheric pressure microwave plasma torch shown in Fig. 2.²⁵ Since this discovery, plasma reactors with different designs have been utilized to create GSG.^{27–31,35,41–43} For example, GSG can be produced through the delivery of ethanol into surface wave-induced microwave plasmas at atmospheric conditions^{28,29,31}

[Fig. 6(a)]. A Torche à Injection Axiale sur Guide d'Ondes (TIAGO)^{44–47} can also generate atmospheric pressure Ar plasmas that are capable of creating GSG.²⁷ A TIAGO consists of a waveguide whose central section is reduced in height [Fig. 6(b)]. Ar plasmas are generated by flowing Ar gas through a hollow metallic rod placed perpendicular to the waveguide in this central section. The introduction of ethanol vapor into the TIAGO results in the deposition of GSG on the walls of the reactor. Another reactor design that is capable of producing GSG consists of a microwave slot antenna connected to a microwave generator [Fig. 6(c)]. Such a reactor can ignite and sustain atmospheric plasmas from an Ar/H₂ gas mixture.³⁵ GSG forms when an aerosol consisting of liquid ethanol and Ar/H₂ is delivered into the reactor using a dual-flow nozzle system and a syringe pump.

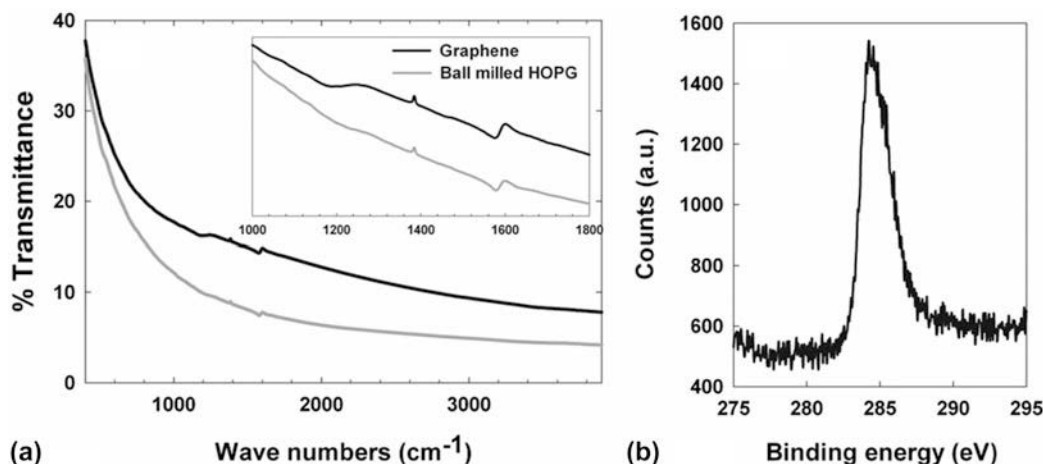


FIG. 5. (a) A Fourier transform infrared spectroscopy spectra of GSG and HOPG. The similar features of the HOPG and GSG between 1000 and 1800 cm^{-1} are shown in the inset. (b) An X-ray photoelectron spectroscopy spectrum of GSG. Reproduced from Ref. 36 with permission from the Royal Society of Chemistry.

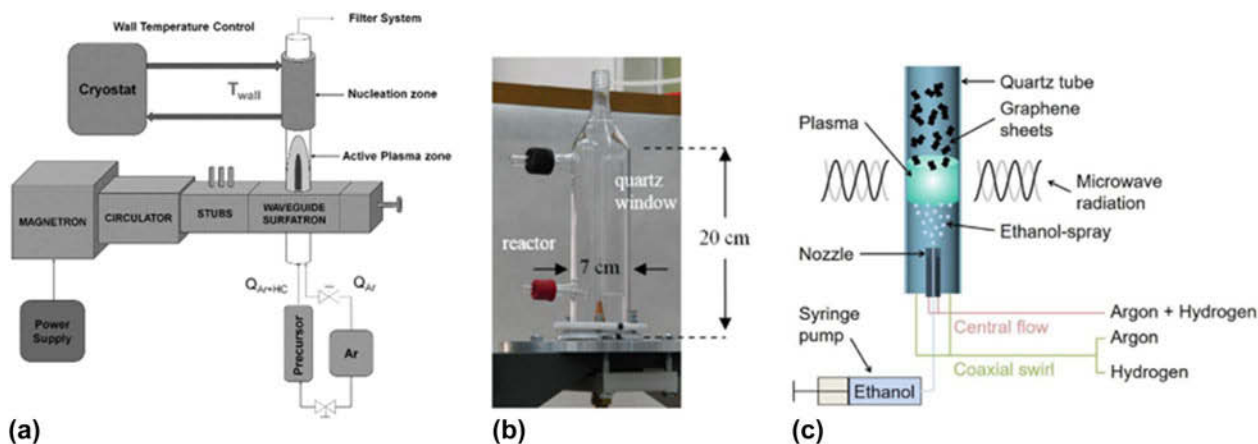


FIG. 6. (a) Schematic of a surface wave-induced microwave plasma reactor. Reproduced from Tatarova et al.: Microwave plasma based single step method for free standing graphene synthesis at atmospheric conditions. *Appl. Phys. Lett.* 103, 134, 101 (2013), with the permission of AIP Publishing. (b) A TIAGO reactor. Reprinted with permission from Ref. 27. (c) Schematic of a microwave slot antenna system. Reprinted from Wiggers et al.: All gas-phase synthesis of graphene: Characterization and its utilization for silicon-based lithium-ion batteries. *Electrochim. Acta* 272, 52–59 (2018), with permission from Elsevier.

The production of GSG using different types of reactors demonstrates that atmospheric pressure plasmas sustained by 2.45 GHz microwave generators create an environment that is conducive to the synthesis of graphene. However, lower reactor pressures are not favorable to the formation of GSG.²⁷ This is because atmospheric plasmas are collisional environments that can achieve the high gas temperatures (3000 K) required for the formation of carbon nanostructures. Collisions between electrons and heavy particles are reduced in sub-atmospheric microwave plasmas, which results in decreased temperatures that prevent the formation of GSG.²⁷ On the other hand, a higher reactor pressure (1.5 atm) has been shown to increase production rates of GSG.³⁵ Despite the increase in GSG formation at higher

pressure, future research should concentrate on optimizing the synthesis of GSG in atmospheric pressure environments because production at ambient conditions will greatly facilitate the large-scale production of the material.

GSG can form over a broad microwave forward power (MFP) range between 250 and 1050 W²⁶ in the plasma torch design shown in Fig. 2. This indicates that the nucleation and growth of GSG do not occur in the coupler region of microwave-generated plasmas.²⁶ Instead, the role of the coupler region in the synthesis process is the dissociation of ethanol into reactive fragments, such as C, C₂, C₂H₂, and H. Indeed, the presence of these fragments in the coupler region has been detected using optical emission spectroscopy during GSG

synthesis experiments.²⁹ The afterglows of plasmas generated by atmospheric plasma torches have been characterized,⁴⁸ and studies have shown that gas temperatures in the afterglow region are not significantly affected by increases in MFP. These results indicate that the fragments created in the coupler region react to form GSG in the plasma afterglow.

However, MFP can have an effect on the synthesized structures in reactors of different design. GSG can be produced in the surface wave reactor shown in Fig. 6(a) at MFPs between 500 and 900 W. Reducing the MFP in this system to 400 W results in the formation of carbon nanoparticles when all other experimental parameters are held constant.³¹ In contrast, TIAGO torches [Fig. 6(b)] operate at lower MFPs than surface wave reactors during GSG production. Thus, the effect of MFP range on GSG formation can vary between reactors of different designs.

The carbon structures that deposit on the walls of various atmospheric plasma reactors provide additional evidence of the effect of reactor design on GSG production. In the surface wave reactor shown in Fig. 6(a), solid materials that deposit on the walls of the reactor are carbonaceous nanoparticles, whereas the materials that exit the reactor are GSG.²⁹ In contrast, Fig. 7 shows that the materials that deposit on the walls of the atmospheric plasma torch shown in Fig. 2 are GSG sheets. These deposits are located between 0 and 100 mm above the coupler region of the reactor. Furthermore, GSG produced in TIAGO reactors [Fig. 6(b)] are collected from reactor walls, which are in close proximity to the Ar plasma.²⁷ The role of the coupler region in atmospheric plasma reactors could be similar from system to system. However, the variation in MFP conditions and the difference in materials deposited on the walls of various reactors suggest that the mechanisms of GSG formation are dependent on reactor design.

B. Precursor composition

GSG forms when liquid ethanol droplets^{25,26,35,36,41} or ethanol vapor^{27–29,31} are delivered into atmospheric Ar

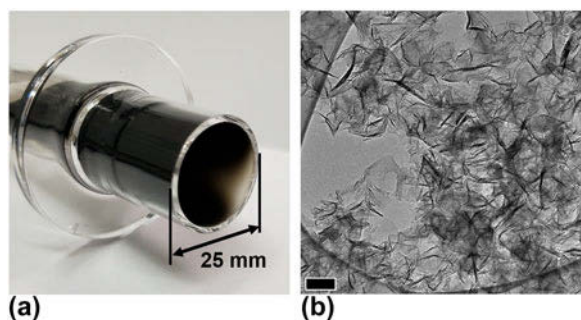


FIG. 7. (a) Solid carbon deposits on the walls of the atmospheric plasma torch shown in Fig. 2. (b) TEM image that shows the deposits are GSG. Scale bar represents 100 nm.

plasmas. It is currently unknown if the phase of ethanol has an effect on the rate of GSG formation. A study that compares GSG production rates when liquid-phase and vapor-phase ethanol are delivered into the same reactor under similar experimental conditions is needed. Initial research into the effects of precursor composition on the formation of GSG investigated the delivery of three precursors into atmospheric plasmas: liquid methanol (CH_4O) droplets, dimethyl ether ($\text{C}_2\text{H}_6\text{O}$) vapor, and liquid isopropanol ($\text{C}_3\text{H}_8\text{O}$) droplets.²⁶ Solid material cannot be obtained with methanol, while isopropanol results in the creation of soot particles instead of GSG. However, GSG can form through the use of dimethyl ether, which is an isomer of ethanol. Therefore, precursor composition has a significant effect on the formation of GSG.

Soot formation from isopropanol provides insight into the mechanisms of solid carbon production in atmospheric Ar plasmas. Soot has been the subject of a large amount of experimental and computational research for decades,⁴⁹ and the prevailing theory of soot formation is that individual particles are formed from polycyclic aromatic hydrocarbon (PAH) nuclei. In both oxidative and non-oxidative environments, PAHs are formed from reactive species such as C_2H_2 , C_3H_3 , and H. PAHs then undergo abstraction by H and subsequently grow through the addition of acetylene molecules. Once formed, PAHs collide and stick to each other to form PAH dimers. The collision of PAH dimers with other PAHs then results in the formation of PAH trimers, PAH tetramers, and so on. As these collisions occur, individual PAH molecules within these clusters grow via chemical reactions at their edges. These processes continue until PAH clusters evolve into individual soot particles. Thus, soot formation in atmospheric plasmas is evidence that reactive fragments, such as C_2H_2 , C, C_2 , and H, are produced in the gas-phase synthesis process.

The lack of solid materials formed through the delivery of methanol further supports this theory, since the compound consists of a single C atom, whereas ethanol, dimethyl ether, and isopropanol contain multiple C atoms. Relative to ethanol, dimethyl ether, and isopropanol, the formation of a C–C bond through the dissociation of methanol is much more of a challenge. The formation of a lower number of C–C bonds can result in less reactive fragments being created, which results in a decreased number of aromatic species. Furthermore, the limited amount of C_2H_2 also hinders the growth of any aromatic rings that do form. Therefore, the formation of a relatively smaller number of PAHs from the dissociation of methanol may prevent the nucleation of a sufficient number of aromatic species and their subsequent growth into solid carbon structures.

A graphene sheet can be thought of as a large PAH molecule. The formation of graphene from ethanol and

dimethyl ether is possibly the result of the slow nucleation of a small number of initial aromatic rings followed by their fast growth into large 2D sheets in the high temperature environment created by an atmospheric plasma.²⁶ Compared with ethanol, the dissociation of isopropanol creates an overabundance of PAHs that subsequently experience multiple collisions with other PAHs to form clusters. These clusters then grow, coagulate, and aggregate to form chains of soot particles.

The gaseous by-products of GSG production have been determined to be H₂ and CO.^{28–30,45,50,51} Thus, the presence of O in alcohols may also affect the structures of the synthesized nanomaterials. GSG produced through the delivery of ethanol contains only 0.1% O.³⁶ This indicates that C and O atoms that are created from the decomposition of ethanol must be reacting to form CO during the gas-phase synthesis process. Methanol consists of a single C atom and a single O atom, and the formation of C–C bonds may compete with the formation of C–O bonds. CO is relatively unreactive, and its formation in the non-oxidative environment of atmospheric Ar plasmas may capture most of the C atoms present, which prevents the formation of C–C bonds and aromatic rings when methanol is used as a precursor. Ethanol and isopropanol each contain a single O atom per multiple C atoms. Even if each O atom bonds with a C atom to form CO, additional C atoms are still available to form C–C bonds.

The ratio of C to H molecules may also have an effect on GSG production. Dimethyl ether, ethanol, methanol, and isopropanol all contain a single O atom. However, GSG can be created through the delivery of ethanol and dimethyl ether, which have a C/H ratio of 0.333. Carbonaceous structures are not produced through the delivery of methanol, which has a C/H ratio of 0.250. Isopropanol, which has a C/H ratio of 0.375, results in soot particles. Therefore, these results indicate that a range of precursor C/H ratios that promote the formation of GSG may exist between the C/H ratios of methanol and isopropanol.

Further research into precursor composition should focus on determining a C/H ratio that maximizes GSG production, as well as elucidating the role of O in the production of GSG. Recently, the delivery of methane (CH₄) into atmospheric Ar plasmas resulted in the production of relatively small amounts of GSG sheets among carbon nanoparticles.⁵² This result suggests that O may not be required for the formation of GSG. A carbon-containing gas, such as acetylene (C₂H₂), could potentially be used to produce GSG since it is a precursor for the formation of aromatic nuclei and does not contain oxygen that results in the creation of CO. The synthesis of GSG through the use of dimethyl ether²⁶ or methane⁵² demonstrates that ethanol is not the sole precursor for GSG formation. Future GSG studies should investigate

the use of gaseous precursors that can facilitate the production of GSG, since the use of gases eliminates the additional time and energy required to atomize or vaporize ethanol.

C. Flow rates of gases and precursors

The residence times of precursors and reactive fragments in atmospheric plasma reactors are strongly affected by the flow rate of the gases used to generate the plasmas. Residence time has a significant influence on the materials produced in the gas-phase synthesis process. A longer residence time that results from a reduction in plasma gas flow rate can enable individual GSG sheets to stack with other sheets to form bulk graphite structures, as well as promote the formation of polyhedral graphitic particles with hollow centers.²⁶

The formation of polyhedral graphitic particles in atmospheric plasmas²⁶ provides additional evidence of the presence of C, C₂, and PAHs in the gas-phase synthesis process. Polyhedral graphitic particles produced by arc discharge have been speculated to originate from carbonaceous clusters that form due to the condensation of C vapor in inert gas atmospheres.^{53–56} These clusters resemble individual spherical soot particles.^{53,54} The clusters grow into larger particles via coagulation and maintain a structural fluidity due to the high temperatures (3500 K) and the bombardment of ions and electrons in the arc discharge.⁵⁴ Because of this fluidity, the particles have been referred to as “liquid carbon droplets.”⁵³ Graphitization of these droplets occurs during cooling, which proceeds from the surface of the particles to the center.^{53,54} Graphite planes are initiated at the outer surface of a particle, and internal planes form and remain parallel to the outer layers as the particle cools.^{53,54} The flat planes of the shells consist of hexagonal rings, and the corners of the particles are a result of pentagonal rings. This graphitization process results in polyhedral graphite particles with hollow centers, which form because the density of graphitized carbon (2.2 g/cm³) is higher than that of amorphous carbon (1.5 g/cm³).^{53,54} The resulting structure minimizes dangling bonds and lowers the energy of the graphite particle.⁵⁴

The flow rate of ethanol can also affect the synthesis of GSG because this factor can increase the mass flux of carbon into atmospheric plasmas.²⁸ Indeed, amorphous carbon structures can be produced instead of GSG in atmospheric plasma reactors by increasing the mass flow rate of ethanol by 600% with all other experimental parameters fixed. The effect of high ethanol flow rates is similar to the effect of using isopropanol as a precursor. Lower flow rates of ethanol result in the formation of a small amount of nuclei surpassing the critical size for nucleation and growth. Conditions in which no supersaturation of species is possible given the limited flux of

carbon promotes the growth of existing nuclei into large GSG sheets rather than the creation of new nuclei.²⁸ An increase in the flux of ethanol results in the creation of more nuclei, which leads to the formation of soot particles.

The current knowledge on the effects of precursor and plasma gas flow rates on GSG formation indicates that it may be possible to produce the material from carbon precursors with compositions that are different from ethanol by changing the residence time. Future studies can determine if GSG forms from isopropanol if the plasma gas flow rate is increased and the flow rate of isopropanol is decreased. Alternatively, an increase in methanol flow rate and decreased plasma gas flow rate could result in GSG formation. The flow rates of gases and precursors have a significant effect on the synthesis of graphene in plasmas and require further study.

IV. THE MAIN CHALLENGE OF GRAPHENE SYNTHESIS IN ATMOSPHERIC PLASMAS

The low rate of production is the main challenge in synthesizing graphene in atmospheric plasmas. GSG has been produced at rates ranging from 10^{-3} to 10^{-1} g/h from a single reactor. Milligram-scale quantities of GSG are sufficient for the research and development of applications in the laboratory. However, the production rate of GSG must be greatly increased for the industrial manufacturing of these applications. Future research into the mechanisms of GSG formation could uncover a plasma reactor design, precursor, and experimental condition that enable a single reactor to achieve a production rate that exceeds 10^1 g/h, which is a rate that has been reported for contemporary top-down processes.⁵⁷

A promising reactor design is the TIAGO torch because it allows for the generation of multiple atmospheric plasmas simultaneously from a single waveguide.^{27,47} A TIAGO system capable of sustaining four atmospheric plasmas has been demonstrated,⁴⁷ and such a system can result in a 4-fold increase in GSG production. Therefore, an array of atmospheric plasmas operating from a single microwave power generator is a viable pathway to industrial GSG production. However, a bottleneck in the TIAGO synthesis process lies in the collection of GSG powder. The deposition of GSG on the walls of an array of TIAGO reactors would necessitate the termination of the production process to procure GSG from reactor walls. A reactor design that employs the parallel plasma generation of the TIAGO design and downstream GSG collection of the plasma torch design could enable the continuous large-scale synthesis of GSG.

To date, a statistical design of experiments (DoE)⁵⁸ aimed at maximizing the production of GSG has not been reported in literature. Single variable tests to determine

the effect of MFP, precursor composition, precursor flow rates, and plasma gas flow rates on GSG have been reported.^{26,28} However, DoE studies could elucidate the influences and interactions of numerous factors on the synthesis of GSG, which could result in the discovery of an experimental condition that maximizes production rate. Much has yet to be learned about the synthesis of graphene in atmospheric plasmas. As the number of researchers investigating GSG increases, so does the possibility of the development of an industrial-scale GSG production process.

V. FEATURES AND POTENTIAL APPLICATIONS OF GSG

A. Purity and structure for TEM imaging and optoelectronics

The pure and highly ordered nature of GSG make it an ideal support film for the TEM imaging of nanomaterials. Atomic resolution imaging of nanoparticles and the direct observation of the interfaces between soft and hard materials have been achieved using GSG as an atomically thin TEM support film.⁵⁹ For example, an enhanced-contrast filtered image of a gold nanoparticle and its surrounding citrate capping layer is shown in Fig. 8(a). This was achieved by blocking the reflections of the underlying GSG support film from the image's digital diffractogram [Fig. 8(a), inset]. The subsequent subtraction of the gold nanoparticle's reflection from the digital diffractogram [Fig. 8(b), inset] enabled the isolated imaging of citrate molecules for the first time [Fig. 8(b)]. In another study, the superior performance of GSG over conventional amorphous carbon support films was demonstrated when GSG was used to image Si nanocrystals and their capping ligands.⁶⁰

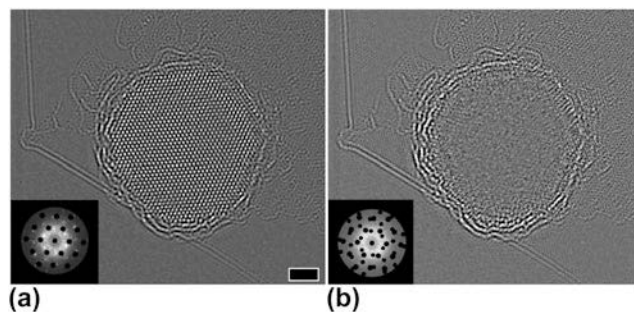


FIG. 8. Graphene-enabled isolation and imaging of citrate molecules. (a) An enhanced-contrast filtered image of the citrate-capped gold nanoparticle. Inset: The graphene reflections were subtracted in a digital diffractogram of the entire image. Scale bar represents 2 nm. (b) An image of the citrate molecules. Inset: The graphene and gold reflections were masked in the digital diffractogram to isolate and image citrate. Reprinted with permission from Lee et al.: Direct imaging of soft–hard interfaces enabled by graphene. *Nano Lett.* 9, 3365 (2009). Copyright 2009 American Chemical Society.

A challenge in using GSG as a TEM support film arises from its crumpled morphology, random orientation of sheets, and the presence of bilayer and few-layer graphene. For nanoparticles to be imaged on GSG, a monolayer region that contains a nanoparticle must be found. This procedure can take considerable time. In contrast, TEM support films fabricated from graphene prepared by the micromechanical cleavage method^{61,62} consist of high-quality monolayer regions with dimensions on the order of tens of micrometers.⁶² Finding nanomaterials on monolayer graphene in these support films is relatively straightforward when compared with GSG.

The advantage of GSG support films over other graphene-coated TEM grids lies in preparation. GSG support films are prepared via a three-step process that involves dispersing GSG in a solvent, depositing a drop of solvent on a conventional TEM grid containing an amorphous support, and allowing the solvent to evaporate. Using this process, dozens of TEM grids can be coated with GSG in minutes. In comparison, it can take hours to micromechanically cleave HOPG, find monolayer graphene on a substrate using optical microscopy, and transfer the graphene to a TEM grid without contaminating it. TEM grids coated with graphene obtained by chemical vapor deposition methods can also take hours to produce, since individual sheets need to be removed from substrates and transferred to TEM grids without contamination.

The purity and structure of GSG also enable the creation of partially fluorinated graphene that exhibits

a band gap. For example, fluorographene was created by reacting GSG with xenon difluoride at 250 °C.⁶³ Pristine graphene does not exhibit a band gap,^{64–66} and near-edge X-ray absorption fine structure (NEXAFS) and photoluminescence (PL) spectroscopy have been used to show that GSG also does not exhibit a band gap.⁶³ The fluorination of GSG changes the pure sp^2 -carbon structure of graphene to a sp^3 -derived carbon–fluorine structure, which results in the formation of a band gap. The NEXAFS and PL measurements shown in Fig. 9 indicate that the band gap of fluorographene is at least 3.8 eV. This band gap is wide enough for optoelectronic applications in the blue/UV spectrum, which means that fluorographene has the potential to be used in electronic, optoelectronic, and energy harvesting applications.⁶³

B. Nanoparticle dispersion for catalysis and energy storage

In addition to improving the TEM characterization of nanomaterials, a GSG sheet can prevent the aggregation of nanoparticles deposited on its surface⁶⁷ and enhance their performance in catalysis and energy storage applications.^{35,41} In a recent study, gold nanoparticles of increasing diameter were dispersed on GSG sheets.⁶⁷ It was discovered that nanoparticles with diameters below 10 nm did not aggregate on GSG and had a tendency to be located on the edges of the sheets [Fig. 10(a)]. This result shows that GSG sheets containing sub-10 nm nanoparticles could potentially be used in catalysis.⁶⁸ A high reactive surface area of catalytic nanoparticles is

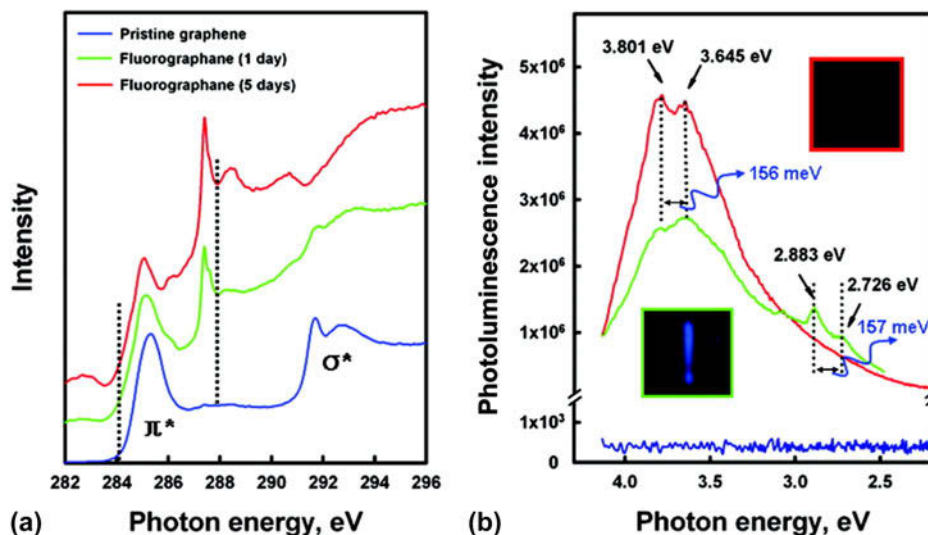


FIG. 9. Band gap opening of fluorographene. (a) NEXAFS spectra of GSG and fluorographene with two different contents of fluorine. The dashed lines at 284.1 and 287.9 eV mark the leading edges of the π^* resonance for the pristine and fluorinated GSG sample, respectively. (b) Room temperature photoluminescence emission of the GSG/fluorographene dispersed in acetone using 290 nm (4.275 eV) excitation. The dotted lines are used for guiding eyes. The interval of dotted line is ~ 156 meV. Optical images (top view) of the blue emission observed after the PL emission was recorded with the samples in 3.5 mL quartz cuvettes. The blue light persists ~ 30 s after the excitation laser is turned off. Reprinted with permission from Jeon et al.: Fluorographene: a wide band gap semiconductor with ultraviolet luminescence. ACS Nano 5, 1042 (2011). Copyright 2011 American Chemical Society.

crucial in catalysis, and the agglomeration of nanoparticles is a problem in this application. GSG can overcome this problem by dispersing sub-10 nm nanoparticles to maximize their surface area.⁶⁷

Indeed, the enhanced catalytic activity of GSG sheets decorated with sub-10 nm Pt nanoparticles has been demonstrated.⁴¹ Pt/GSG composites [Fig. 10(b)] have been prepared and used as a direct methanol fuel cell electrocatalyst.⁴¹ Cyclic voltammetry measurements showed that GSG sheets containing 20 wt% Pt nanoparticles exhibited superior catalytic activity toward the oxidation of methanol compared with commercially available Pt/C composites [Fig. 11(a)], which was attributed to the dispersion of Pt nanoparticles on GSG and the high conductivity of the GSG sheets. Furthermore, these Pt/GSG composites outperformed other composites

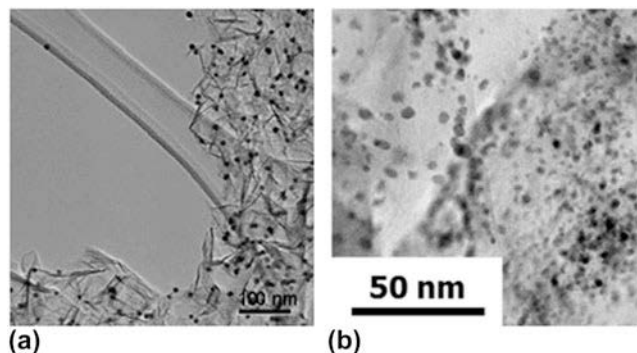


FIG. 10. Nanoparticles supported by GSG. (a) 10 nm gold nanoparticles on GSG. Reprinted with permission from Ref. 67. (b) Platinum nanoparticles on GSG. Reprinted with permission from Ref. 41.

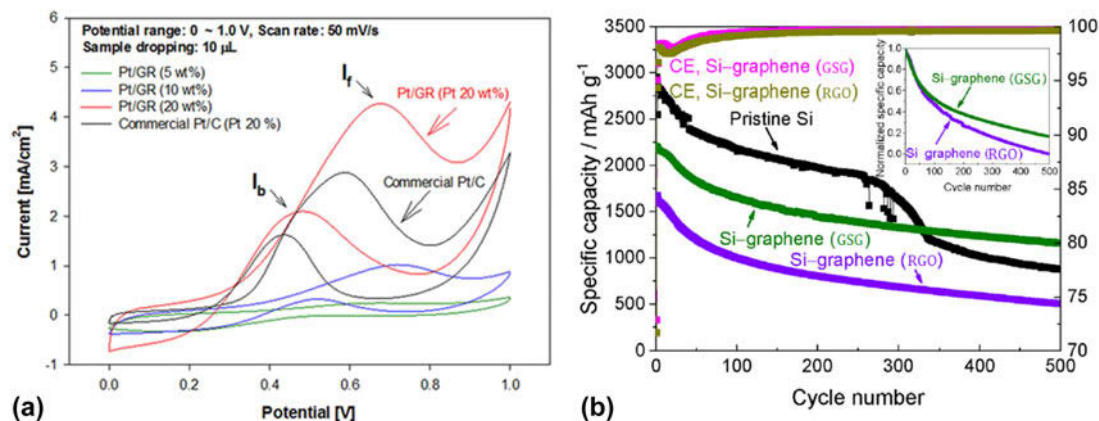


FIG. 11. (a) Cyclic voltammetry measurements for methanol oxidation reaction catalyzed by commercial Pt/C (carbon black) and Pt/GSG composite in the mixture solution of 0.05 M H₂SO₄ + 1 M CH₃OH within the potential range of 0–1.0 V. Reprinted with permission from Ref. 41. (b) Galvanostatic cycling performance of pristine Si, Si-GSG, and Si-RGO composites measured at 0.5 C charge/discharge. Delithiation/lithiation and the Coulombic efficiency of Si-GSG and Si-RGO composites are shown in comparison with pristine silicon nanoparticles. The first two cycles for all materials were carried out at 0.025 C for lithiation and 0.05 C for delithiation and 0.1 C (for all lithiation and delithiation), respectively. The inset shows the normalized data for Si-GSG and Si-RGO clearly indicating the superior long-term stability of the Si-GSG composite. Reprinted from Wiggers et al.: All gas-phase synthesis of graphene: Characterization and its utilization for silicon-based lithium-ion batteries. *Electrochim. Acta* 272, 52–59 (2018), with permission from Elsevier.

consisting of Pt and graphene produced by the reduction of graphene oxide in the methanol oxidation reaction.⁴¹

GSG sheets containing Si nanoparticles have been used as Li-ion battery anodes.³⁵ Relative to anodes consisting of pristine Si nanoparticles and composite anodes consisting of Si nanoparticles and reduced graphene oxide (RGO), GSG can significantly enhance the long-term stability and Coulomb efficiency of anodes consisting of Si nanoparticles dispersed on GSG sheets [Fig. 11(b)].

Thus, GSG can disperse nanoparticles on its surface and can also have a synergistic effect with the nanomaterials. However, there is a size limit to the dispersive capability of GSG, since gold nanoparticles larger than 50 nm in diameter did not disperse in GSG but rather aggregated randomly throughout the sheets.⁶⁷ Additional research is needed to determine the limits of the dispersive capability of GSG. Furthermore, the performance of GSG in a number of graphene–nanoparticle composite applications is unknown. For example, GSG–copper nanoparticle composites could potentially be used in electrochemical sensing of carbohydrates⁶⁹ and GSG sheets decorated with silver nanoparticles could be used in molecularly selective surface-enhanced Raman scattering.⁷⁰

C. Graphitic nanocrystals for lubrication

The morphology of crumpled graphene has been compared with that of crumpled paper.^{43,52} However, GSG may be crumpled because of the presence of graphitic nanocrystals in the synthesized sheets.⁷¹ In situ TEM has revealed that graphitic nanocrystals provide

GSG with additional mechanical stability, enable the material to reversibly deform, and prevent GSG from being flattened like paper.⁷¹ Graphitic nanocrystals, such as the one circled in Fig. 12(a), are defined as features on a GSG sheet consisting of small, dark needle-like regions. These features are rigid and do not change structurally during the deformation of GSG.

Figure 12 shows a series of in situ TEM images that demonstrate the reversible deformation of GSG. The initial form of a GSG sheet with a nanocrystal as it makes contact with an atomic force microscopy (AFM) tip is shown in Fig. 12(a). Figures 12(b) and 12(c) show how the sheet folds into itself as it slides past the AFM tip. However, the graphitic nanocrystal maintains the sheet's structure during this process. As shown in Fig. 12(d), the rigid nanocrystal enables the GSG sheet to revert back to its original form when it detaches from the AFM tip. A graphical model of this process is shown in Figs. 12(e)–12(h). This phenomenon was reproducible, and the results demonstrate that the folding and unfolding of crumpled GSG is reversible.

The nanocrystals that maintain the morphology of GSG can make the sheets useful in lubrication applications, where a crumpled morphology has been shown to prevent aggregation and re-stacking in lubricant oils.¹³ Aggregation is a great challenge for ultrafine particle additives in lubricant oils because the phenomenon reduces effective particle concentrations, prevents particles from entering the working area of surfaces, and results in unstable tribological performance.¹³ Indeed, the deliberate crumpling of flat graphene into graphene balls causes the crumpled material to self-disperse in oils.¹³ Lubricants containing graphene balls exhibit lower coefficients of friction and reduced wear

compared with oils containing flat graphene flakes, carbon black nanoparticles, or graphite powder.¹³ It is therefore possible that the use of crumpled GSG as an additive in lubricant oils will result in self-dispersion of the powder and enhancements in the tribological properties of the oil.

D. Rotational stacking for electrical applications

GSG sheets that consist of more than a single graphene layer can exhibit rotational stacking instead of Bernal stacking.^{72,73} Aberration-corrected TEM images of bilayer and few-layer GSG have revealed unambiguous Moiré patterns in the sheets.⁷² These patterns are similar to the rotational stacking faults that have been observed in few-layer graphene obtained from graphite.⁷⁴

The rotational stacking of GSG layers is interesting for two reasons. First, bilayer and few-layer GSG sheets may not always be stacking in the standard AB Bernal packing of bulk graphite during synthesis. The number of layers and quality of GSG could be controlled through process conditions, such as residence time in the reactor. Multi-layer graphite particles with standard AB stacking, with an interlayer distance of 0.335 nm, could be created by reducing the flow rate of the Ar gas used to generate atmospheric plasmas.²⁶ Future studies on GSG should focus on determining process conditions that could control the stacking of few-layer sheets. Second, GSG powders consisting of single-, bi-, and few-layer graphene may exhibit enhanced properties when compared with graphene powders obtained from graphite. This is because bilayer and few-layer graphene with rotational stacking faults can have electrical properties similar to monolayer graphene,^{75,76} as well as distinct thermal properties.^{77,78}

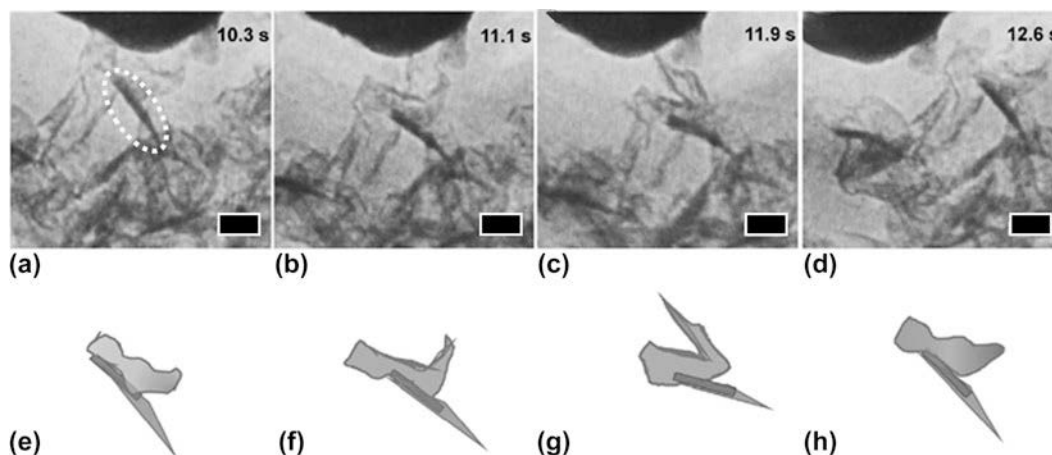


FIG. 12. Folding and unfolding of GSG. (a) A crumpled GSG sheet with a graphitic nanocrystal (circled) making contact with an AFM tip. (b and c) The GSG sheet was moving from left to right in this sequence, while the AFM tip was stationary. The GSG sheet with nanocrystal folded as it maintained contact with the AFM tip. The nanocrystal remained rigid and did not change structurally. (d) The GSG sheet rapidly reverted to its initial configuration as it detached from the AFM tip. (e–h) Graphical models showing the structural changes that occurred as the sheet was sliding against the tip. Scale bars: 50 nm. Reprinted from Marks et al.: In situ observations of graphitic staples in crumpled graphene. Carbon 132, 760 (2018), with permission from Elsevier.

It could therefore be possible that various electrical and thermal applications of graphene could be enhanced through the use of GSG because of the material's purity, structure, and rotational disorder. This theory is supported by recent studies that showed that pellets consisting of GSG had an electrical conductivity of 4751 S/m, while pellets consisting of RGO had a lower conductivity of 3057 S/m.³⁵ Currently, the effect of process conditions, such as plasma gas flow rate, on the electrical properties of GSG is currently unknown and should be studied. Future research into GSG should also investigate the performance of the material in electrical applications, such as electrically conductive inks and polymers.

VI. GSG PRODUCTION COMPARED WITH OTHER PLASMA-BASED METHODS

A. Free-standing graphene obtained through PECVD

Free-standing graphene sheets can be synthesized using PECVD techniques.^{79–81} For example, graphene can form and grow vertically on various substrates (e.g., Si, W, Al₂O₃) using radio frequency (13.56 MHz) PECVD and methane as a precursor.^{79,80} Low-pressure microwave reactors can also be utilized to produce vertically aligned “carbon nanowalls” with an average thickness of several nanometers using copper substrates and a precursor mixture of acetylene and ammonia.⁸²

Vertically grown graphene sheets produced by PECVD have a similar appearance and Raman spectrum as GSG.⁷⁹ However, there are three major differences between PECVD-grown graphene and GSG. First, the production of GSG is a substrate-free process, while substrates are necessary in PECVD. Substrate temperature can also affect the structure of PECVD-grown sheets, and high-quality specimens require substrate temperatures above 630 °C.⁷⁹ Second, GSG is created under ambient conditions, while graphene growth by PECVD requires low reactor pressures (12 Pa for radio frequency PECVD^{79,80} and 1300 Pa for microwave PECVD⁸²). Third, the synthesis of GSG is a continuous process that proceeds indefinitely as long as a plasma is maintained and precursors are supplied. The environmental conditions of PECVD reactors require the synthesis processes to be stopped in order to return to ambient conditions to harvest the free-standing graphene. Despite the similarities in structure and quality, the synthesis of graphene in atmospheric plasmas has a number of advantages over the nucleation and growth of free-standing graphene sheets by PECVD.

B. Large-area graphene films created through PECVD

The formation of GSG in atmospheric plasmas proceeds via gas-phase reactions. In contrast, the large and

flat graphene films deposited on substrates by PECVD depend on surface reactions. Graphene growth on a nickel substrate begins with the decomposition of a carbonaceous precursor, such as methane, in a low-pressure (0.12 Pa) plasma reactor.⁸³ The free carbon that results from the decomposition process dissolves in nickel to form a solid solution.^{84–86} The cooling of the solid solution is a critical step because the solubility of carbon in nickel decreases as the temperature in the reactor is lowered. Cooling at a rate of 10 °C/s^{85,87} causes carbon atoms to dissolve out of the solid solution and precipitate on the nickel surface to form large-area graphene films with lateral dimensions on the order of centimeters.⁸³ The formation of graphene films on copper substrates can be achieved through the catalytic decomposition of methane on the copper surface, which is a self-limiting process.⁸⁸ Compared with nickel, copper has a much lower carbon solubility. Once a copper surface is covered with graphene, no further growth occurs because there is no longer any catalyst exposed to hydrocarbons in the plasma reactor and only a small amount of carbon dissolves in copper.⁸⁸

The differences between GSG and large-area graphene films deposited on substrates are similar to the disparities between GSG and PECVD-produced free-standing graphene flakes. Low pressures (<5 Pa) and high substrate temperatures (>300 °C) are required to create graphene films on copper and nickel. However, there are additional differences between the atmospheric plasma production of GSG and graphene films synthesized by PECVD. The nucleation and growth of graphene by PECVD involve surface reactions, and thus the quality of the underlying substrate can affect the quality of the synthesized films. The deposition of pure and highly ordered monolayer graphene requires high-quality substrates, which can lead to greatly increased production costs. Additionally, substrate treatments are required prior to deposition. The exposure of substrates to plasmas in order to remove surface contamination and increase grain size requires additional time and energy, which further increases the time and cost of PECVD synthesis.⁸⁹

The main advantage of PECVD-grown graphene over GSG is size. GSG powder consists of randomly oriented and crumpled sheets with sizes ranging from hundreds of nanometers to micrometers, while PECVD-grown films can grow to centimeter scale. Continuous and highly ordered PECVD graphene films are suitable for the fabrication of electronic devices.⁹⁰ However, the use of graphene films in applications for graphene powder (e.g., nanocomposites, conductive inks, lubrication) can be costly and time-consuming, since additional steps are needed to extract graphene films from substrates. These steps can include coating the graphene with a polymer support, chemical etching of the underlying nickel or copper substrate, removing the polymer support, and

transferring the graphene to a desired application.^{91,92} These transfer processes are time-consuming and can contaminate and generate defects on graphene films, which diminish the properties of the material.⁹⁰ In comparison, pure and highly ordered GSG can be used immediately after synthesis for graphene powder applications.

VII. GSG COMPARED WITH GRAPHENE PRODUCED BY TOP-DOWN TECHNIQUES

A. Creating graphene from graphite

Graphene was first isolated and studied through the micromechanical cleavage method.⁶⁶ This process produces pristine graphene flakes that are not contaminated with oxygen. However, micromechanical cleavage is time-consuming and the yield of monolayer flakes is extremely small, which makes the technique only suitable for fundamental research purposes.⁹³ Two widely used methods that have been developed for the production of bulk quantities of graphene powder are the reduction of graphene oxide^{94–98} and liquid-phase exfoliation.^{19,99–108} This section will compare the production and quality of GSG with those of RGO and liquid-phase exfoliated graphene (LPEG). The differences between GSG, RGO, and LPEG are summarized in Table I.

B. Comparison of production rates, requirements, and by-products

Production rate is the main advantage of RGO and LPEG over GSG. As shown in Table I, rates of production greater than 10^1 g/h have been reported for graphene obtained through top-down methods.⁵⁷ In comparison, 10^{-1} g/h is the maximum production rate that has been reported for graphene produced in atmospheric plasmas.³⁵ Furthermore, the production of LPEG and RGO is scalable, and kilogram quantities of RGO flakes are now commercially available.

The synthesis of GSG in atmospheric plasmas has the advantages of lower production requirements and reduced environmental impact. For instance, the creation of RGO involves multiple steps and large volumes of

hazardous chemicals that can negatively impact the environment. The oxidation of graphite and the subsequent reduction of graphene oxide requires chemicals such as nitric acid, sulfuric acid, sodium hydroxide, hydrazine, dimethylhydrazine, and sodium borohydride.^{94,98,109} These chemicals can produce hazardous gases and pose a risk of explosion.¹⁰⁹ Large volumes of purified water are also required throughout the production of RGO, and wastewater from the process can contain mixed acids and heavy metal ions.¹⁰⁹ Even the most recent studies reporting the rapid synthesis of graphene oxide and RGO utilize acids and large volumes of water to produce the materials.^{57,109}

Similarly, the LPEG production process requires multiple steps, significant water, and hazardous chemicals. A number of liquid-phase exfoliation techniques use chemicals such as sulfuric acid,^{110,111} nitric acid,¹⁰⁶ chlorohydric acid,¹⁰¹ and CrO_3 ¹⁰¹ to prepare graphite for exfoliation. Significant quantities of solvent are then needed to exfoliate expanded graphite and to purify and disperse LPEG.¹¹¹ Current liquid-phase exfoliation techniques require at least 1 ton of solvent to disperse 1 kg of graphene,¹¹¹ which is neither beneficial to the environment nor economically feasible. Reducing the amount of solvent used in LPEG production results in the re-stacking of monolayer flakes by van der Waals interactions. A non-dispersion strategy was recently developed to enable the mass production of graphene slurries, but even this method requires multiple steps, hazardous chemicals, and large amounts of water just to produce gram-scale quantities of graphene.¹¹¹ Once produced, LPEG is typically stored in a solvent or water,¹¹¹ and the use of LPEG powder in a number of graphene applications requires techniques to separate flakes from solvents, such as filtration.^{101,106,108,111} Once separated from solvent, LPEG powder must be washed with purified water to remove any residual chemicals from the flakes.^{101,103,106,110}

In contrast to top-down methods of graphene production, the synthesis of graphene in atmospheric plasmas only requires a microwave plasma reactor, Ar gas, and a carbon-containing precursor. GSG is highly stable at ambient conditions,³⁵ can be stored indefinitely in its dry as-synthesized state, and can be used immediately for graphene applications. GSG can also be produced with a lower impact to the environment than RGO and LPEG because plasma reactors can be powered using sustainable energy (e.g., wind and solar) and precursors for GSG formation (e.g., ethanol and dimethyl ether) can be obtained from renewable resources.^{112,113}

Unlike the liquid chemical waste that is generated during the production of RGO and LPEG, the by-products of the gas-phase synthesis process are H_2 and CO. These gaseous by-products can be harvested and used in a number of useful applications. For instance, H_2

TABLE I. Comparison of the production rates, composition, and quality of GSG, RGO, and LPEG.

	Production rate (g/h)	Ref.	Composition (mass%)			Quality			
			C	H	O	Ref.	I_G/I_D	I_{2D}/I_G	Ref.
GSG	0.1	35	98.9	1	0.1	36	4.8	1.4	27
RGO	>10	57	86.4	0.8	11.3	116	0.8	0.3	57
LPEG	>10	101	90.5	0.8	8.4	111	3.6	0.4	111

is considered a nonpolluting and efficient energy carrier that has the potential to be used in future clean energy technologies, such as fuel cells for vehicles.^{50,114} Currently, the two primary technologies of producing H₂ are the catalytic route through the water gas shift reaction and the electrolytic decomposition of water.⁵⁰ Indeed, the delivery of ethanol into atmospheric plasmas has been investigated as a method of H₂ production.^{44,45} Thus, compared with RGO and LPEG production, the synthesis of GSG is safer and more environmentally friendly, and the by-products of the gas phase process can be useful in other applications.

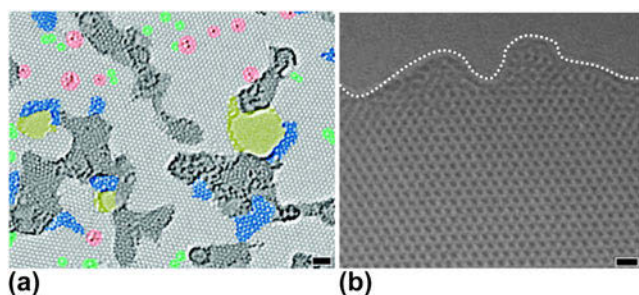


FIG. 13. (a) TEM image of RGO with color added. Pristine areas and contaminated regions are light and dark gray, respectively. Blue regions are disordered networks or topological defects that are caused by the oxidation reduction process. Red areas are adatoms or substitutions. Green and yellow areas are isolated topological defects and holes, respectively. Scale bar: 1 nm. Reprinted with permission from Gomez-Navarro et al.: Atomic structure of RGO. *Nano Lett.* 10, 1144 (2010). Copyright 2010 American Chemical Society. (b) A TEM image of pure and highly ordered GSG. The dashed line indicates the edge of the sheet. Scale bar: 0.4 nm. Reproduced from Ref. 36 with permission from The Royal Society of Chemistry.

C. Comparison of the structure and quality of GSG, RGO, and LPEG

RGO is derived from graphite oxide, which is a highly defective form of graphite with a disrupted sp^2 bonding network.¹⁹ Therefore, RGO does not possess the mechanical, electrical, and thermal properties of graphene created by the micromechanical cleavage of HOPG. As shown in Fig. 13(a), the intrinsic structure of RGO exhibits contamination, topological defects, disordered networks, adatoms, and holes, which all significantly diminish the properties of graphene.¹¹⁵ Figure 13(b) shows that the highly ordered arrangement of sp^2 -bonded carbon atoms of GSG extends throughout the sheet, which does not have holes, disorder, and contamination.³⁶ Furthermore, the complete reduction of graphene oxide to pure graphene has not been accomplished. As shown in Table I, RGO sheets typically have a mass composition of 86.4% C, 0.8% H, and 11.3% O.¹¹⁶ In contrast, GSG sheets have a composition of 98.9% C, 1.0% H, and 0.1% O.³⁶ Side-by-side Raman spectroscopy characterization of RGO and GSG [Fig. 14(a)] shows that the I_G/I_D ratio of RGO is much lower compared to that of GSG, which further proves that the disorder in the structure of RGO is significantly higher than GSG.³⁵ Raman peak ratios that can be used to compare the quality of GSG and RGO are summarized in Table I.

GSG also has the advantage of being higher in quality than LPEG. LPEG is produced from flake graphite,^{105,111} which contains numerous localized defects in its structure.^{94,95} LPEG also contains a relatively high amount of oxygen. As shown in Table I, LPEG flakes have a mass composition of 90.5% C, 0.8% H, and 8.4% O.¹¹¹ Furthermore, Table I shows that the peaks in the Raman

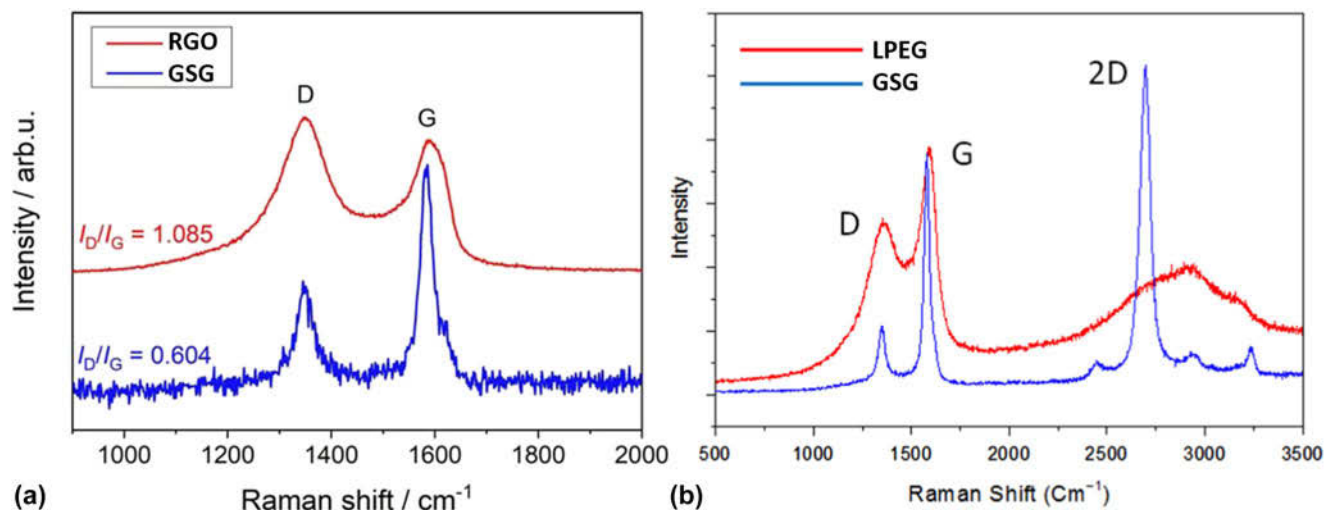


FIG. 14. (a) Raman spectra of RGO and GSG. Reprinted from Wiggers et al.: All gas-phase synthesis of graphene: Characterization and its utilization for silicon-based lithium-ion batteries. *Electrochim. Acta* 272, 52–59 (2018), with permission from Elsevier. (b) Raman spectra of LPEG and GSG. Reprinted with permission from Ref. 27.

spectra of LPEG typically have I_{2D}/I_G ratios that are less than 0.5,^{105,111} which is an indicator of multiple graphene layers. The multilayer nature of LPEG flakes is also evident in the side-by-side comparison of LPEG and GSG Raman spectra shown in Fig. 14(b). GSG has a sharp, symmetric 2D peak characteristic of graphene, while LPEG has a 2D peak shape that is an indicator of multilayer graphene.³⁷ Thus, GSG is closer in quality to pristine graphene than LPEG.

VIII. CONCLUSION

Graphene can be rapidly and continuously produced in atmospheric plasmas without the need for substrates, catalysts, or acids. The single-step gas-phase synthesis process involves the delivery of a carbon-containing precursor directly into a microwave-generated Ar plasma that can decompose organic compounds into their atomic elements due to the high average energies of its electrons and heavy particles. Reactive species combine in the high temperature environment of the plasma afterglow to form graphene, H_2 , and CO. The graphene that is produced by this process is pure, highly ordered, and stable under ambient conditions.

Future research should investigate the performance of GSG in applications for graphene powder. RGO has been used in a myriad of applications, such as high-strength nanocomposites,^{117,118} energy storage,^{20,24} water purification,^{119,120} and drug delivery.¹²¹ However, it is currently unknown if the pure and highly ordered nature of GSG will enhance the mechanical properties of nanocomposites, increase the energy storage capabilities of batteries, or improve the tribological properties of lubricants. It is worth noting that the synthesis of graphene in atmospheric plasmas was first reported in 2008,²⁵ but other research groups did not start producing and studying GSG until 2013.³¹ GSG research has gradually increased over the last five years. The initial studies into the properties and applications of GSG are promising. Laboratory-scale quantities of GSG are being produced by a growing number of research groups worldwide, and it is therefore likely that the performance of GSG in various applications will be reported in the foreseeable future.

The greatest challenge in producing GSG using atmospheric plasmas is the low rate of production. GSG production rates are miniscule compared with the industrial quantities of RGO and LPEG that are currently on the market. Therefore, future research into GSG should focus on increasing the yield of gas-phase synthesis methods. This will require further investigations into the nucleation and growth processes occurring in atmospheric plasmas. A better understanding of GSG synthesis mechanisms will enable the determination of an optimal reactor design for industrial production, process conditions that produce a higher percentage of single-

layer graphene, and carbon-containing precursors that are both lower in cost and renewable.

REFERENCES

1. C. Lee, X. Wei, J.W. Kysar, and J. Hone: Measurement of the elastic properties and intrinsic strength of monolayer graphene. *Science* **321**, 385 (2008).
2. F. Liu, P. Ming, and J. Li: Ab initio calculation of ideal strength and phonon instability of graphene under tension. *Phys. Rev. B* **76**, 064120 (2007).
3. D.J. Celentano, E.E. Cabezas, C.M. García, and A.E. Monsalve: Characterization of the mechanical behaviour of materials in the tensile test: Experiments and simulation. *Modell. Simul. Mater. Sci. Eng.* **12**, S425 (2004).
4. K.L. Murty, M.D. Mathew, Y. Wang, V.N. Shah, and F.M. Haggag: Nondestructive determination of tensile properties and fracture toughness of cold worked A36 steel. *Int. J. Pressure Vessels Piping* **75**, 831 (1998).
5. S. Ghosh, I. Calizo, D. Teweldebrhan, E.P. Pokatilov, D.L. Nika, A.A. Balandin, W. Bao, F. Miao, and C.N. Lau: Extremely high thermal conductivity of graphene: Prospects for thermal management applications in nanoelectronic circuits. *Appl. Phys. Lett.* **92**, 151911 (2008).
6. K.M.F. Shahil and A.A. Balandin: Thermal properties of graphene and multilayer graphene: Applications in thermal interface materials. *Solid State Commun.* **152**, 1331 (2012).
7. X. Du, I. Skachko, A. Barker, and E.Y. Andrei: Approaching ballistic transport in suspended graphene. *Nat. Nanotechnol.* **3**, 491 (2008).
8. K.I. Bolotin, K.J. Sikes, Z. Jiang, M. Klima, G. Fudenberg, J. Hone, P. Kim, and H.L. Stormer: Ultrahigh electron mobility in suspended graphene. *Solid State Commun.* **146**, 351 (2008).
9. R.J. Young, I.A. Kinloch, L. Gong, and K.S. Novoselov: The mechanics of graphene nanocomposites: A review. *Compos. Sci. Technol.* **72**, 1459 (2012).
10. Y. Wang, J. Yu, W. Dai, Y. Song, D. Wang, L. Zeng, and N. Jiang: Enhanced thermal and electrical properties of epoxy composites reinforced with graphene nanoplatelets. *Polym. Compos.* **36**, 556 (2015).
11. Y.-L. Li, C.-F. Kuan, C.-H. Chen, H.-C. Kuan, M.-C. Yip, S.-L. Chiu, and C.-L. Chiang: Preparation, thermal stability and electrical properties of PMMA/functionalized graphene oxide nanosheets composites. *Mater. Chem. Phys.* **134**, 677 (2012).
12. M. Shtein, R. Nativ, M. Buzaglo, K. Kahil, and O. Regev: Thermally conductive graphene-polymer composites: Size, percolation, and synergy effects. *Chem. Mater.* **27**, 2100 (2015).
13. X. Dou, A.R. Koltonow, X. He, H.D. Jang, Q. Wang, Y.W. Chung, and J. Huang: Self-dispersed crumpled graphene balls in oil for friction and wear reduction. *Proc. Natl. Acad. Sci. U. S. A.* **113**, 1528 (2016).
14. L. Huang, Y. Huang, J. Liang, X. Wan, and Y. Chen: Graphene-based conducting inks for direct inkjet printing of flexible conductive patterns and their applications in electric circuits and chemical sensors. *Nano Res.* **4**, 675 (2011).
15. V. Dua, S.P. Surwade, S. Ammu, S.R. Agnihotra, S. Jain, K.E. Roberts, S. Park, R.S. Ruoff, and S.K. Manohar: All-organic vapor sensor using inkjet-printed reduced graphene oxide. *Angew. Chem., Int. Ed. Engl.* **49**, 2154 (2010).
16. E.B. Secor, B.Y. Ahn, T.Z. Gao, J.A. Lewis, and M.C. Hersam: Rapid and versatile photonic annealing of graphene inks for flexible printed electronics. *Adv. Mater.* **27**, 6683 (2015).
17. E.B. Secor, P.L. Prabhuramirashi, K. Puntambekar, M.L. Geier, and M.C. Hersam: Inkjet printing of high conductivity, flexible graphene patterns. *J. Phys. Chem. Lett.* **4**, 1347 (2013).

18. F. Torrisi, T. Hasan, W. Wu, Z. Sun, A. Lombardo, T.S. Kulmala, G.W. Hsieh, S. Jung, F. Bonaccorso, P.J. Paul, D. Chu, and A.C. Ferrari: Inkjet-printed graphene electronics. *ACS Nano* **6**, 2992 (2012).
19. R. Raccichini, A. Varzi, S. Passerini, and B. Scrosati: The role of graphene for electrochemical energy storage. *Nat. Mater.* **14**, 271 (2014).
20. J. Zhu, D. Yang, Z. Yin, Q. Yan, and H. Zhang: Graphene and graphene-based materials for energy storage applications. *Small* **10**, 3480 (2014).
21. O.A. Vargas C., A. Caballero, and J. Morales: Can the performance of graphene nanosheets for lithium storage in Li-ion batteries be predicted? *Nanoscale* **4**, 2083 (2012).
22. J. Hassoun, F. Bonaccorso, M. Agostini, M. Angelucci, M.G. Betti, R. Cingolani, M. Gemmi, C. Mariani, S. Panero, V. Pellegrini, and B. Scrosati: An advanced lithium-ion battery based on a graphene anode and a lithium iron phosphate cathode. *Nano Lett.* **14**, 4901 (2014).
23. Y. Zhu, S. Murali, M.D. Stoller, K.J. Ganesh, W. Cai, P.J. Ferreira, A. Pirkle, R.M. Wallace, K.A. Cychoz, M. Thommes, D. Su, E.A. Stach, and R.S. Ruoff: Carbon-based supercapacitors produced by activation of graphene. *Science* **332**, 1537 (2011).
24. M.D. Stoller, S. Park, Y. Zhu, J. An, and R.S. Ruoff: Graphene-based ultracapacitors. *Nano Lett.* **8**, 3498 (2008).
25. A. Dato, V. Radmilovic, Z. Lee, J. Phillips, and M. Frenklach: Substrate-free gas-phase synthesis of graphene sheets. *Nano Lett.* **8**, 2012 (2008).
26. A. Dato and M. Frenklach: Substrate-free microwave synthesis of graphene: Experimental conditions and hydrocarbon precursors. *New J. Phys.* **12**, 125013 (2010).
27. C. Melero, R. Rincón, J. Muñoz, G. Zhang, S. Sun, A. Perez, O. Royuela, C. González-Gago, and M.D. Calzada: Scalable graphene production from ethanol decomposition by microwave argon plasma torch. *Plasma Phys. Controlled Fusion* **60**, 014009 (2018).
28. E. Tatarova, A. Dias, J. Henriques, A.M.B.d. Rego, A.M. Ferraria, M.V. Abrashev, C.C. Luhrs, J. Phillips, F.M. Dias, and C.M. Ferreira: Microwave plasmas applied for the synthesis of free standing graphene sheets. *J. Phys. D: Appl. Phys.* **47**, 385501 (2014).
29. D. Tsyganov, N. Bundaleska, E. Tatarova, A. Dias, J. Henriques, A. Rego, A. Ferraria, M.V. Abrashev, F.M. Dias, C.C. Luhrs, and J. Phillips: On the plasma-based growth of 'flowing' graphene sheets at atmospheric pressure conditions. *Plasma Sources Sci. Technol.* **25**, 015013 (2016).
30. R. Rincón, C. Melero, M. Jiménez, and M.D. Calzada: Synthesis of multi-layer graphene and multi-wall carbon nanotubes from direct decomposition of ethanol by microwave plasma without using metal catalysts. *Plasma Sources Sci. Technol.* **24**, 032005 (2015).
31. E. Tatarova, J. Henriques, C.C. Luhrs, A. Dias, J. Phillips, M.V. Abrashev, and C.M. Ferreira: Microwave plasma based single step method for free standing graphene synthesis at atmospheric conditions. *Appl. Phys. Lett.* **103**, 134101 (2013).
32. S.D. Berger, D.R. McKenzie, and P.J. Martin: EELS analysis of vacuum arc-deposited diamond-like films. *Philos. Mag. Lett.* **57**, 285 (1988).
33. A. Duarte-Moller, F. Espinosa-Magaña, R. Martínez-Sánchez, M. Avalos-Borja, G.A. Hirata, and L. Cota-Araiza: Study of different forms of carbon by analytical electron microscopy. *J. Electron Spectrosc. Relat. Phenom.* **104**, 61 (1999).
34. P.K. Chu and L. Li: Characterization of amorphous and nanocrystalline carbon films. *Mater. Chem. Phys.* **96**, 253 (2006).
35. A. Münzer, L. Xiao, Y.H. Sehlleier, C. Schulz, and H. Wiggers: All gas-phase synthesis of graphene: Characterization and its utilization for silicon-based lithium-ion batteries. *Electrochim. Acta* **272**, 52 (2018).
36. A. Dato, Z. Lee, K.J. Jeon, R. Erni, V. Radmilovic, T.J. Richardson, and M. Frenklach: Clean and highly ordered graphene synthesized in the gas phase. *Chem. Commun.* **40**, 6095–7 (2009).
37. A.C. Ferrari, J.C. Meyer, V. Scardaci, C. Casiraghi, M. Lazzeri, F. Mauri, S. Piscanec, D. Jiang, K.S. Novoselov, S. Roth, and A.K. Geim: Raman spectrum of graphene and graphene layers. *Phys. Rev. Lett.* **97**, 187401 (2006).
38. F. Tuinstra and J.L. Koenig: Raman spectrum of graphite. *J. Chem. Phys.* **53**, 1126 (1970).
39. L.M. Malard, M.A. Pimenta, G. Dresselhaus, and M.S. Dresselhaus: Raman spectroscopy in graphene. *Phys. Rep.* **473**, 51 (2009).
40. J.C. Meyer, A.K. Geim, M.I. Katsnelson, K.S. Novoselov, T.J. Booth, and S. Roth: The structure of suspended graphene sheets. *Nature* **446**, 60 (2007).
41. E.H. Jo, H. Chang, S.K. Kim, J.H. Choi, S.R. Park, C.M. Lee, and H.D. Jang: One-step synthesis of Pt/graphene composites from Pt acid dissolved ethanol via microwave plasma spray pyrolysis. *Sci. Rep.* **6**, 33236 (2016).
42. A. Dias, N. Bundaleski, E. Tatarova, F.M. Dias, M. Abrashev, U. Cvelbar, O.M.N.D. Teodoro, and J. Henriques: Production of N-graphene by microwave N₂-Ar plasma. *J. Phys. D: Appl. Phys.* **49**, 055307 (2016).
43. E. Tatarova, A. Dias, J. Henriques, M. Abrashev, N. Bundaleska, E. Kovacevic, N. Bundaleski, U. Cvelbar, E. Valcheva, B. Arnaudov, A.M.B. do Rego, A.M. Ferraria, J. Berndt, E. Felizardo, O. Teodoro, T. Strunskus, L.L. Alves, and B. Gonçalves: Towards large-scale in free-standing graphene and N-graphene sheets. *Sci. Rep.* **7**, 10175 (2017).
44. R. Rincón, A. Marinas, J. Muñoz, and M.D. Calzada: Hydrogen production from ethanol decomposition by microwave plasma TIAGO torch. *Int. J. Hydrogen Energy* **39**, 11441 (2014).
45. R. Rincón, M. Jiménez, J. Muñoz, M. Sáez, and M.D. Calzada: Hydrogen production from ethanol decomposition by two microwave atmospheric pressure plasma sources: Surfatron and TIAGO torch. *Plasma Chem. Plasma Process.* **34**, 145 (2013).
46. R. Rincón, J. Muñoz, M. Sáez, and M.D. Calzada: Spectroscopic characterization of atmospheric pressure argon plasmas sustained with the Torche à Injection Axiale sur Guide d'Ondes. *Spectrochim. Acta, Part B* **81**, 26 (2013).
47. M. Moisan, Z. Zakrzewski, and J.C. Rostaing: Waveguide-based single and multiple nozzle plasma torches: The TIAGO concept. *Plasma Sources Sci. Technol.* **10**, 387 (2001).
48. C-K. Chen and J. Phillips: Impact of aerosol particles on the structure of an atmospheric pressure microwave plasma afterglow. *J. Phys. D: Appl. Phys.* **35**, 998 (2002).
49. M. Frenklach: Reaction mechanism of soot formation in flames. *Phys. Chem. Chem. Phys.* **4**, 2028 (2002).
50. M. Jiménez, R. Rincón, A. Marinas, and M.D. Calzada: Hydrogen production from ethanol decomposition by a microwave plasma: Influence of the plasma gas flow. *Int. J. Hydrogen Energy* **38**, 8708 (2013).
51. M. Jiménez, C. Yubero, and M.D. Calzada: Study on the reforming of alcohols in a surface wave discharge (SWD) at atmospheric pressure. *J. Phys. D: Appl. Phys.* **41**, 175201 (2008).
52. N. Bundaleska, D. Tsyganov, A. Dias, E. Felizardo, J. Henriques, F.M. Dias, M. Abrashev, J. Kissovski, and E. Tatarova: Microwave plasma enabled synthesis of free standing carbon nanostructures at atmospheric pressure conditions. *Phys. Chem. Chem. Phys.* **20**, 13810 (2018).
53. D. Ugarte: Onion-like graphitic particles. *Carbon* **33**, 989 (1995).

54. Y. Saito, T. Yoshikawa, M. Inagaki, M. Tomita, and T. Hayashi: Growth and structure of graphitic tubules and polyhedral particles in arc-discharge. *Chem. Phys. Lett.* **204**, 277 (1993).
55. P.M. Ajayan, P. Redlich, and M. Rühle: Balance of graphite deposition and multishell carbon nanotube growth in the carbon arc discharge. *J. Mater. Res.* **12**, 244 (2011).
56. D. Ugarte: Morphology and structure of graphitic soot particles generated in arc-discharge C60 production. *Chem. Phys. Lett.* **198**, 596 (1992).
57. S. Abdolhosseinzadeh, H. Asgharzadeh, and H. Seop Kim: Fast and fully-scalable synthesis of reduced graphene oxide. *Sci. Rep.* **5**, 10160 (2015).
58. S.A. Weissman and N.G. Anderson: Design of experiments (DoE) and process optimization. A review of recent publications. *Org. Process Res. Dev.* **19**, 1605 (2014).
59. Z. Lee, K.J. Jeon, A. Dato, R. Erni, T.J. Richardson, M. Frenklach, and V. Radmilovic: Direct imaging of soft-hard interfaces enabled by graphene. *Nano Lett.* **9**, 3365 (2009).
60. M.G. Panthani, C.M. Hessel, D. Reid, G. Casillas, M. José-Yacamán, and B.A. Korgel: Graphene-supported high-resolution TEM and STEM imaging of silicon nanocrystals and their capping ligands. *J. Phys. Chem. C* **116**, 22463 (2012).
61. J.C. Meyer, C. Kisielowski, R. Erni, M.D. Rossell, M.F. Crommie, and A. Zettl: Direct imaging of lattice atoms and topological defects in graphene membranes. *Nano Lett.* **8**, 3582 (2008).
62. J.C. Meyer, C.O. Girit, M. Crommie, and A. Zettl: Imaging and dynamics of light atoms and molecules on graphene. *Nature* **454**, 319 (2008).
63. K.J. Jeon, Z. Lee, E. Pollak, L. Moreschini, A. Bostwick, C.M. Park, R. Mendelsberg, V. Radmilovic, R. Kostecki, T.J. Richardson, and E. Rotenberg: Fluorographene: A wide band gap semiconductor with ultraviolet luminescence. *ACS Nano* **5**, 1042 (2011).
64. A.K. Geim and K.S. Novoselov: The rise of graphene. *Nat. Mater.* **6**, 183 (2007).
65. K.S. Novoselov, A.K. Geim, S.V. Morozov, D. Jiang, M.I. Katsnelson, I.V. Grigorieva, S.V. Dubonos, and A.A. Firsov: Two-dimensional gas of massless Dirac fermions in graphene. *Nature* **438**, 197 (2005).
66. K.S. Novoselov, A.K. Geim, S.V. Morozov, D. Jiang, Y. Zhang, S.V. Dubonos, I.V. Grigorieva, and A.A. Firsov: Electric field effect in atomically thin carbon films. *Science* **306**, 666 (2004).
67. K.J. Jeon and Z. Lee: Size-dependent interaction of Au nanoparticles and graphene sheet. *Chem. Commun.* **47**, 3610 (2011).
68. J.M. Planeix, N. Coustel, B. Coq, V. Brotons, P.S. Kumbhar, R. Dutartre, P. Geneste, P. Bernier, and P.M. Ajayan: Application of carbon nanotubes as supports in heterogeneous catalysis. *J. Am. Chem. Soc.* **116**, 7935 (1994).
69. Q. Chen, L. Zhang, and G. Chen: Facile preparation of graphene-copper nanoparticle composite by in situ chemical reduction for electrochemical sensing of carbohydrates. *Anal. Chem.* **84**, 171 (2012).
70. S. Murphy, L. Huang, and P.V. Kamat: Reduced graphene oxide-silver nanoparticle composite as an active SERS material. *J. Phys. Chem. C* **117**, 4740 (2013).
71. A.Y.W. Lin, X-x. Yu, A. Dato, G. Krauss, and L.D. Marks: In situ observations of graphitic staples in crumpled graphene. *Carbon* **132**, 760 (2018).
72. G.H. Ryu, H.J. Park, N.Y. Kim, and Z. Lee: Atomic resolution imaging of rotated bilayer graphene sheets using a low kV aberration-corrected transmission electron microscope. *Appl. Microsc.* **42**, 218 (2012).
73. Z. Lee, A. Dato, K.J. Jeon, R. Erni, T.J. Richardson, M. Frenklach, and V. Radmilovic: Atomic resolution imaging and spectroscopy of graphene using the TEAM 0.5. *Microsc. Microanal.* **15**, 124 (2009).
74. J.H. Warner, M.H. Rummeli, T. Gemming, B. Buchner, and G.A. Briggs: Direct imaging of rotational stacking faults in few layer graphene. *Nano Lett.* **9**, 102 (2009).
75. F. Varchon, P. Mallet, L. Magaud, and J-Y. Veuillen: Rotational disorder in few-layer graphene films on 6H-SiC(000-1): A scanning tunneling microscopy study. *Phys. Rev. B* **77**, 165415 (2008).
76. J. Hass, F. Varchon, J.E. Millan-Otoya, M. Sprinkle, N. Sharma, W.A. de Heer, C. Berger, P.N. First, L. Magaud, and E.H. Conrad: Why multilayer graphene on 4H-SiC(000-1) behaves like a single sheet of graphene. *Phys. Rev. Lett.* **100**, 125504 (2008).
77. H. Li, H. Ying, X. Chen, D.L. Nika, A.I. Cocemasov, W. Cai, A.A. Balandin, and S. Chen: Thermal conductivity of twisted bilayer graphene. *Nanoscale* **6**, 13402 (2014).
78. D.L. Nika, A.I. Cocemasov, and A.A. Balandin: Specific heat of twisted bilayer graphene: Engineering phonons by atomic plane rotations. *Appl. Phys. Lett.* **105**, 031904 (2014).
79. J. Wang, M. Zhu, R.A. Outlaw, X. Zhao, D.M. Manos, and B.C. Holloway: Synthesis of carbon nanosheets by inductively coupled radio-frequency plasma enhanced chemical vapor deposition. *Carbon* **42**, 2867 (2004).
80. J.J. Wang, M.Y. Zhu, R.A. Outlaw, X. Zhao, D.M. Manos, B.C. Holloway, and V.P. Mammana: Free-standing subnanometer graphite sheets. *Appl. Phys. Lett.* **85**, 1265 (2004).
81. B.L. French, J.J. Wang, M.Y. Zhu, and B.C. Holloway: Structural characterization of carbon nanosheets via X-ray scattering. *J. Appl. Phys.* **97**, 114317 (2005).
82. A.T.H. Chuang, B.O. Boskovic, and J. Robertson: Freestanding carbon nanowalls by microwave plasma-enhanced chemical vapour deposition. *Diamond Relat. Mater.* **15**, 1103 (2006).
83. G. Nandamuri, S. Roumimov, and R. Solanki: Remote plasma assisted growth of graphene films. *Appl. Phys. Lett.* **96**, 154101 (2010).
84. L.G. De Arco, Z. Yi, A. Kumar, and Z. Chongwu: Synthesis, transfer, and devices of single- and few-layer graphene by chemical vapor deposition. *IEEE Trans. Nanotechnol.* **8**, 135 (2009).
85. K.S. Kim, Y. Zhao, H. Jang, S.Y. Lee, J.M. Kim, K.S. Kim, J.H. Ahn, P. Kim, J.Y. Choi, and B.H. Hong: Large-scale pattern growth of graphene films for stretchable transparent electrodes. *Nature* **457**, 706 (2009).
86. A. Reina, X. Jia, J. Ho, D. Nezich, H. Son, V. Bulovic, M.S. Dresselhaus, and J. Kong: Large area, few-layer graphene films on arbitrary substrates by chemical vapor deposition. *Nano Lett.* **9**, 30 (2009).
87. Q. Yu, J. Lian, S. Siriponglert, H. Li, Y.P. Chen, and S-S. Pei: Graphene segregated on Ni surfaces and transferred to insulators. *Appl. Phys. Lett.* **93**, 113103 (2008).
88. Y. Zhang, L. Zhang, and C. Zhou: Review of chemical vapor deposition of graphene and related applications. *Acc. Chem. Res.* **46**, 2329 (2013).
89. T. Yamada, J. Kim, M. Ishihara, and M. Hasegawa: Low-temperature graphene synthesis using microwave plasma CVD. *J. Phys. D: Appl. Phys.* **46**, 063001 (2013).
90. D.G. Papageorgiou, I.A. Kinloch, and R.J. Young: Mechanical properties of graphene and graphene-based nanocomposites. *Prog. Mater. Sci.* **90**, 75 (2017).
91. X. Li, W. Cai, J. An, S. Kim, J. Nah, D. Yang, R. Piner, A. Velamakanni, I. Jung, E. Tutuc, S.K. Banerjee, L. Colombo, and R.S. Ruoff: Large-area synthesis of high-quality and uniform graphene films on copper foils. *Science* **324**, 1312 (2009).
92. S. Bae, H. Kim, Y. Lee, X. Xu, J.S. Park, Y. Zheng, J. Balakrishnan, T. Lei, H.R. Kim, Y.I. Song, Y.J. Kim,

- K.S. Kim, B. Ozyilmaz, J.H. Ahn, B.H. Hong, and S. Iijima: Roll-to-roll production of 30-inch graphene films for transparent electrodes. *Nat. Nanotechnol.* **5**, 574 (2010).
93. X.-Y. Wang, A. Narita, and K. Müllen: Precision synthesis versus bulk-scale fabrication of graphenes. *Nat. Rev. Chem.* **2**, 0100 (2017).
94. D.R. Dreyer, S. Park, C.W. Bielawski, and R.S. Ruoff: The chemistry of graphene oxide. *Chem. Soc. Rev.* **39**, 228 (2010).
95. M. Wissler: Graphite and carbon powders for electrochemical applications. *J. Power Sources* **156**, 142 (2006).
96. W.S. Hummers and R.E. Offeman: Preparation of graphitic oxide. *J. Am. Chem. Soc.* **80**, 1339 (1958).
97. D. Li, M.B. Muller, S. Gilje, R.B. Kaner, and G.G. Wallace: Processable aqueous dispersions of graphene nanosheets. *Nat. Nanotechnol.* **3**, 101 (2008).
98. S. Park and R.S. Ruoff: Chemical methods for the production of graphenes. *Nat. Nanotechnol.* **4**, 217 (2009).
99. M. Cai, D. Thorpe, D.H. Adamson, and H.C. Schniepp: Methods of graphite exfoliation. *J. Mater. Chem.* **22**, 24992 (2012).
100. Y. Hernandez, V. Nicolosi, M. Lotya, F.M. Blighe, Z. Sun, S. De, I.T. McGovern, B. Holland, M. Byrne, Y.K. Gun'Ko, J.J. Boland, P. Niraj, G. Duesberg, S. Krishnamurthy, R. Goodhue, J. Hutchison, V. Scardaci, A.C. Ferrari, and J.N. Coleman: High-yield production of graphene by liquid-phase exfoliation of graphite. *Nat. Nanotechnol.* **3**, 563 (2008).
101. S. Lin, L. Dong, J. Zhang, and H. Lu: Room-temperature intercalation and ~1000-fold chemical expansion for scalable preparation of high-quality graphene. *Chem. Mater.* **28**, 2138 (2016).
102. J.N. Coleman: Liquid exfoliation of defect-free graphene. *Acc. Chem. Res.* **46**, 14 (2013).
103. D. Nuvoli, L. Valentini, V. Alzari, S. Scognamillo, S.B. Bon, M. Piccinini, J. Illescas, and A. Mariani: High concentration few-layer graphene sheets obtained by liquid phase exfoliation of graphite in ionic liquid. *J. Mater. Chem.* **21**, 3428 (2011).
104. U. Khan, A. O'Neill, M. Lotya, S. De, and J.N. Coleman: High-concentration solvent exfoliation of graphene. *Small* **6**, 864 (2010).
105. K.R. Paton, E. Varrla, C. Backes, R.J. Smith, U. Khan, A. O'Neill, C. Boland, M. Lotya, O.M. Istrate, P. King, T. Higgins, S. Barwich, P. May, P. Puczkarski, I. Ahmed, M. Moebius, H. Pettersson, E. Long, J. Coelho, S.E. O'Brien, E.K. McGuire, B.M. Sanchez, G.S. Duesberg, N. McEvoy, T.J. Pennycook, C. Downing, A. Crossley, V. Nicolosi, and J.N. Coleman: Scalable production of large quantities of defect-free few-layer graphene by shear exfoliation in liquids. *Nat. Mater.* **13**, 624 (2014).
106. P.L. Chiu, D.D. Mastrogiovanni, D. Wei, C. Louis, M. Jeong, G. Yu, P. Saad, C.R. Flach, R. Mendelsohn, E. Garfunkel, and H. He: Microwave- and nitronium ion-enabled rapid and direct production of highly conductive low-oxygen graphene. *J. Am. Chem. Soc.* **134**, 5850 (2012).
107. D. Wei, L. Grande, V. Chundi, R. White, C. Bower, P. Andrew, and T. Ryhanen: Graphene from electrochemical exfoliation and its direct applications in enhanced energy storage devices. *Chem. Commun.* **48**, 1239 (2012).
108. V. Leon, A.M. Rodriguez, P. Prieto, M. Prato, and E. Vazquez: Exfoliation of graphite with triazine derivatives under ball-milling conditions: Preparation of few-layer graphene via selective noncovalent interactions. *ACS Nano* **8**, 563 (2014).
109. S. Pei, Q. Wei, K. Huang, H.M. Cheng, and W. Ren: Green synthesis of graphene oxide by seconds timescale water electrolytic oxidation. *Nat. Commun.* **9**, 145 (2018).
110. A.M. Dimiev, G. Ceriotti, A. Metzger, N.D. Kim, and J.M. Tour: Chemical mass production of graphene nanoplatelets in approximately 100% yield. *ACS Nano* **10**, 274 (2016).
111. L. Dong, Z. Chen, X. Zhao, J. Ma, S. Lin, M. Li, Y. Bao, L. Chu, K. Leng, H. Lu, and K.P. Loh: A non-dispersion strategy for large-scale production of ultra-high concentration graphene slurries in water. *Nat. Commun.* **9**, 76 (2018).
112. S. Kumar, N. Singh, and R. Prasad: Anhydrous ethanol: A renewable source of energy. *Renewable Sustainable Energy Rev.* **14**, 1830 (2010).
113. T.A. Semelsberger, R.L. Borup, and H.L. Greene: Dimethyl ether (DME) as an alternative fuel. *J. Power Sources* **156**, 497 (2006).
114. E. Tatarova, N. Bundaleska, J.P. Sarrette, and C.M. Ferreira: Plasmas for environmental issues: From hydrogen production to 2D materials assembly. *Plasma Sources Sci. Technol.* **23**, 063002 (2014).
115. C. Gomez-Navarro, J.C. Meyer, R.S. Sundaram, A. Chuvilin, S. Kurasch, M. Burghard, K. Kern, and U. Kaiser: Atomic structure of reduced graphene oxide. *Nano Lett.* **10**, 1144 (2010).
116. H.C. Schniepp, J.L. Li, M.J. McAllister, H. Sai, M. Herrera-Alonso, D.H. Adamson, R.K. Prud'homme, R. Car, D.A. Saville, and I.A. Aksay: Functionalized single graphene sheets derived from splitting graphite oxide. *J. Phys. Chem. B* **110**, 8535 (2006).
117. M.A. Rafiee, J. Rafiee, Z. Wang, H. Song, Z.Z. Yu, and N. Koratkar: Enhanced mechanical properties of nanocomposites at low graphene content. *ACS Nano* **3**, 3884 (2009).
118. J.R. Potts, D.R. Dreyer, C.W. Bielawski, and R.S. Ruoff: Graphene-based polymer nanocomposites. *Polymer* **52**, 5 (2011).
119. V. Chandra, J. Park, Y. Chun, J.W. Lee, I.-C. Hwang, and K.S. Kim: Water-dispersible magnetite-reduced graphene oxide composites for arsenic removal. *ACS Nano* **4**, 3979 (2010).
120. S. Homaeigohar and M. Elbahri: Graphene membranes for water desalination. *NPG Asia Mater.* **9**, e427 (2017).
121. H. Kim, D. Lee, J. Kim, T.I. Kim, and W.J. Kim: Photothermally triggered cytosolic drug delivery via endosome disruption using a functionalized reduced graphene oxide. *ACS Nano* **7**, 6735 (2013).